

Structures of μ O-conotoxins from *Conus marmoreus*

INHIBITORS OF TETRODOTOXIN (TTX)-SENSITIVE AND TTX-RESISTANT SODIUM CHANNELS IN MAMMALIAN SENSORY NEURONS*[§]

Received for publication, December 1, 2003, and in revised form, March 24, 2004
Published, JBC Papers in Press, March 24, 2004, DOI 10.1074/jbc.M313002200

Norelle L. Daly^{‡§}, Jenny A. Ekberg^{‡§¶}, Linda Thomas[‡], David J. Adams[¶], Richard J. Lewis^{¶¶},
and David J. Craik^{‡***}

From the [‡]Institute for Molecular Bioscience and [¶]School of Biomedical Sciences, University of Queensland, Brisbane, 4072 Queensland, Australia

The μ O-conotoxins are an intriguing class of conotoxins targeting various voltage-dependent sodium channels and molluscan calcium channels. In the current study, we have shown MrVIA and MrVIB to be the first known peptidic inhibitors of the transient tetrodotoxin-resistant (TTX-R) Na⁺ current in rat dorsal root ganglion neurons, in addition to inhibiting tetrodotoxin-sensitive Na⁺ currents. Human TTX-R sodium channels are a therapeutic target for indications such as pain, highlighting the importance of the μ O-conotoxins as potential leads for drug development. Furthermore, we have used NMR spectroscopy to provide the first structural information on this class of conotoxins. MrVIA and MrVIB are hydrophobic peptides that aggregate in aqueous solution but were solubilized in 50% acetonitrile/water. The three-dimensional structure of MrVIB consists of a small β -sheet and a cystine knot arrangement of the three-disulfide bonds. It contains four backbone "loops" between successive cysteine residues that are exposed to the solvent to varying degrees. The largest of these, loop 2, is the most disordered part of the molecule, most likely due to flexibility in solution. This disorder is the most striking difference between the structures of MrVIB and the known δ - and ω -conotoxins, which along with the μ O-conotoxins are members of the O superfamily. Loop 2 of ω -conotoxins has previously been shown to contain residues critical for binding to voltage-gated calcium channels, and it is interesting to speculate that the flexibility observed in MrVIB may accommodate binding to both sodium and molluscan calcium channels.

Conotoxins are of great interest as ligands in neuroscience and are valuable leads in drug design based on their specificity and potency for therapeutically relevant receptors and ion

channels (1, 2). Several subtypes of one such ion channel, the sodium channel, have been implicated in clinical states, including pain (3–6), stroke (7, 8), and epilepsy (9, 10). Consequently, conotoxins targeting voltage-gated sodium channels are not only important for further characterization of the channel but may themselves be useful as therapeutics.

The μ O-conotoxins, MrVIA and MrVIB from the venom of *Conus marmoreus* (11), are a particularly interesting family of conotoxins, because they block voltage-sensitive sodium channels (VSSC)¹ but also interact with the calcium channel in molluscan neurons. MrVIA and MrVIB have been shown to block tetrodotoxin (TTX)-resistant (TTX-R) Na⁺ current in molluscan neurons (11), the TTX-sensitive (TTX-S) Na⁺ current through Na_v1.2 expressed in *Xenopus* oocytes, and the TTX-S Na⁺ current in hippocampal neurons (12). Despite the high sequence conservation between MrVIA and MrVIB (only three residues differ) the peptides behave differently at the calcium channel in molluscan neurons. At low micromolar concentrations, MrVIA acts as a calcium channel agonist, whereas MrVIB acts as an antagonist. However, at higher doses both toxins block the fast-inactivating calcium channel. This cross-channel activity observed for μ O-conotoxins has been suggested to represent an "intermediate" variant of conotoxin in the diversification of one conotoxin structural family (13).

Comparison of the μ O-conotoxins with other conotoxins targeting either sodium or calcium channels highlights some striking differences as well as similarities. Although the μ -conotoxins target VSSCs and contain three disulfide bonds, the similarities to the μ O-conotoxins appear to end there. Apart from the cysteine residues there is no sequence homology, and the spacings between the cysteine residues are significantly different, as shown in Fig. 1. Furthermore, MrVIA inhibits mammalian VSSCs through a novel mechanism distinct from site 1 targeted by the μ -conotoxins, saxitoxin, and tetrodotoxin (12).

The μ O-conotoxins show greater similarities to both the ω - and δ -conotoxins than to the μ -conotoxins. These similarities involve the spacings between the cysteine residues (Fig. 1) and similar precursor sequences, and consequently all three families have been placed in the O superfamily (11). Although the sequence homology in the mature peptides is restricted to the

* This work was supported in part by a grant from the Australian Research Council (to D. J. C., R. J. L., and D. J. A.). The costs of publication of this article were defrayed in part by the payment of page charges. This article must therefore be hereby marked "advertisement" in accordance with 18 U.S.C. Section 1734 solely to indicate this fact.

[§] The on-line version of this article (available at <http://www.jbc.org>) contains Table S1.

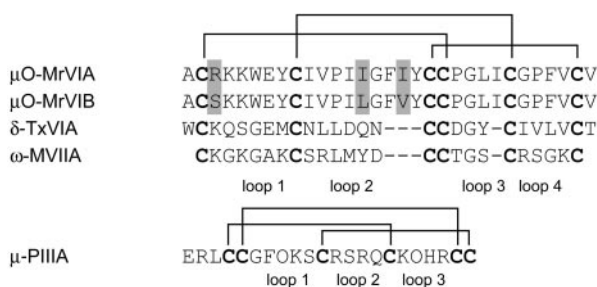
The atomic coordinates and structure factors (code 1RMK) have been deposited in the Protein Data Bank, Research Collaboratory for Structural Bioinformatics, Rutgers University, New Brunswick, NJ (<http://www.rcsb.org/>).

[¶] Both authors contributed equally to this work.

^{¶¶} To whom correspondence may be addressed. Tel.: 61-7-3346-2109; Fax: 61-7-3346-2029; E-mail: rlewis@imb.uq.edu.au.

^{***} An Australian Research Council Senior Fellow. To whom correspondence may be addressed. Tel.: 61-7-3346-2109; Fax: 61-7-3346-2029; E-mail: d.craik@imb.uq.edu.au.

¹ The abbreviations used are: VSSC, voltage-sensitive sodium channels; CSI, chemical shift index; DQF-COSY, double-quantum-filtered correlation spectroscopy; DRG, dorsal root ganglia; ECOSY, exclusive correlation spectroscopy; MS, mass spectrometry; NOE, nuclear Overhauser effect; NOESY, two-dimensional NOE spectroscopy; r.m.s.d., root mean square deviation; HPLC, reversed-phase high performance liquid chromatography; TOCSY, two-dimensional total correlation spectroscopy; TTX-R, tetrodotoxin-resistant; TTX-S, tetrodotoxin-sensitive; TEA, tetraethylammonium; ICK, inhibitor cystine knot.



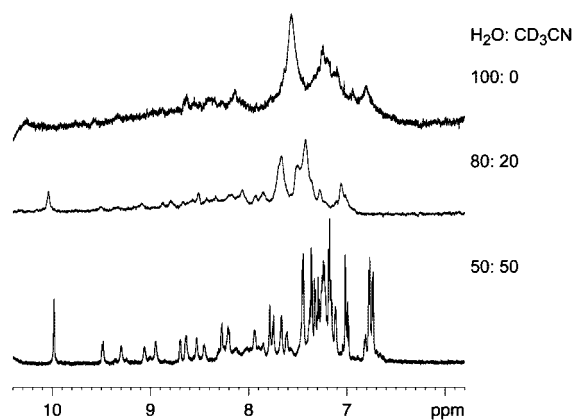


FIG. 2. ^1H NMR spectra of MrVIB. One-dimensional spectra were recorded in H_2O , 20% CD_3CN , and 50% CD_3CN on a 750-MHz spectrometer at 290 K.

The extracellular solution contained (in mM): 140 TEA-Cl, 4 BaCl_2 , 10 D-glucose, 10 HEPES-TEA-OH, pH 7.3. In all solutions, osmolarity was adjusted to 290–300 mosM with sucrose. Toxins were applied via a gravity-fed perfusion system. μO -conotoxins MrVIA and MrVIB were dissolved in bath solution containing $\leq 0.01\%$ Me_2SO . Me_2SO at this concentration had no effects on Na^+ currents.

Data Analysis—All data were analyzed using Clampfit 8 software (Axon Instruments Inc., Union city, CA). Tetrodotoxin (TTX)-resistant Na^+ currents were recorded in the presence of ≥ 300 nM TTX, at least 5 min following bath perfusion. Cells that contained $\geq 90\%$ current that was abolished by application of 300 nM TTX were used to study toxin effects on TTX-S Na^+ current. In this case, TTX was applied at the beginning of the experiment to classify the Na^+ current and then washed out. Data are expressed as means \pm S.E. with n indicating the number of neurons used. Concentration-response curves were analyzed using GraphPad Prism 2.0 (San Diego, CA) and fitted with a one-site binding equation, $Y = 1/(1 + 10^{(\alpha - \log EC_{50})})$. K_D values for kinetic experiments were calculated using the following formulas: $K_D = K_{\text{off}}/K_{\text{on}}$ (M), where $*K_{\text{off}} = 1/\tau_{\text{off}} \text{ s}^{-1}$ and $*K_{\text{on}} = 1/(\tau_{\text{on}} - K_{\text{off}}[\text{toxin}]) \text{ M}^{-1} \cdot \text{s}^{-1}$. K_{off} and K_{on} were calculated from single exponential functions fitted to the time-course curves using GraphPad Prism 2.0.

RESULTS

A preliminary analysis of MrVIA and MrVIB using NMR spectroscopy revealed broad signals in aqueous solutions, indicative of aggregation. A range of pH values and temperatures did not improve the quality of the NMR spectra, but titration with acetonitrile had a beneficial effect, as illustrated in Fig. 2. The titration was carried out from 0 to 90% aqueous acetonitrile, but the highest quality spectra were observed at 50%, and the peptides were insoluble in 100% acetonitrile. Methanol titrations were also performed but did not enhance the quality of the spectra. Both MrVIA and MrVIB behaved in a similar manner, and further structural studies were performed only on MrVIB.

Assignments of the NMR spectra of MrVIB were made using two-dimensional homonuclear methods (22), and the ^1H chemical shifts are supplied as supplementary material. Chemical shifts in the amide region are generally well dispersed, and the relatively large number of resolved cross-peaks in the NOESY spectrum allowed determination of a well defined structure for most regions of the molecule. Interestingly, the amide proton of the N-terminal alanine is visible in the TOCSY spectrum, suggesting that it is involved in long-lived hydrogen bonds or is otherwise protected from exchanging with the solvent. Peaks from terminal amino groups are not normally observed in NMR spectra of peptides.

There are four backbone loops between successive cysteine residues of the μO -conotoxins, as shown in Fig. 1. The residues in loop 2, the largest of the four loops, display significantly fewer NOEs than the other parts of the molecule. Furthermore,

one residue in this loop, Leu¹⁴, and the amide proton of Cys²⁰ were not visible in the spectra and therefore could not be assigned. Several residues gave stronger cross-peaks in the TOCSY spectra recorded at 308 K compared with those recorded at 290 K, including Cys⁹, Phe¹⁶, and Tyr¹⁸. However, in general the quality of the NOESY spectra was better at lower temperatures, and thus structures were calculated from the data recorded at 290 K.

Secondary Structure of MrVIB—Trends in the observed chemical shifts provided a useful first insight into the secondary structure of MrVIB. Chemical shift indices (CSI (23)) for the backbone α -protons were calculated using the measured chemical shifts, and random coil values (24) and are illustrated in Fig. 3. Several of the residues have chemical shifts that differ from the random coil values by more than 0.1 ppm and hence have CSI values of ± 1 , but there are no significant stretches of either positive or negative CSI values, suggesting that the structure is not dominated by either helices or β -sheets.

From a consideration of the experimental NOE, slow exchange and coupling patterns illustrated in Fig. 3, together with some longer range NOEs between backbone protons, an indication of the likely secondary structure was derived and is schematically illustrated in Fig. 4. The major secondary structural element is a β -sheet involving residues 24–25 and 30–31. The presence of $\alpha_{\text{H}(i-1)}-\delta_{\text{H}i}$ NOE signals and the absence of $\alpha_{\text{H}(i-1)}-\alpha_{\text{H}i}$ NOE signals in the NOESY spectrum for all three proline residues (Pro¹², Pro²¹, and Pro²⁷) confirms that their X-Pro peptide bonds are in the *trans* conformation. It is not uncommon that proline residues have *cis* peptide bonds when adjacent to aromatic residues (25). This does not appear to be the case for MrVIB, because, although Phe²⁸ follows Pro²⁷, the peptide bond between Gly²⁶ and Pro²⁷ is in the *trans* conformation. However, Phe²⁸ adopts a positive phi angle that is presumably necessary to stabilize this region of the molecule.

After completion of the assignments for the 50% acetonitrile/water data, spectra at lower acetonitrile concentrations were re-examined. These spectra showed fewer peaks than in 50% acetonitrile, due to the broadening/disappearance of certain residues. For example, in the spectra recorded at 25% acetonitrile/water several residues from loop 2 are not visible. The absence of signals from residues in loop 2 suggests that they are broadened, possibly as a result of intermediate exchange between multiple conformations. These conformers may reflect intermolecular interactions associated with the aggregation observed in aqueous solution.

Structure Determination—Solution structures for MrVIB were determined using simulated annealing, including experimental distance restraints and dihedral angle restraints. Of the final 50 calculated structures, the 20 lowest energy structures consistent with experimental data were chosen to represent the family of MrVIB solution structures as shown in Fig. 5. The disulfide bond connectivities used in the structure calculations were those reported by McIntosh *et al.* (11) (Cys²-Cys²⁰, Cys⁹-Cys²⁵, and Cys¹⁹-Cys³⁰). They were determined using chemical synthesis with a selective protection strategy for two of the cysteine residues.

A summary of the structural statistics for this family is given in Table I. The structures are in agreement with the experimental data, with no distance violation exceeding 0.3 Å and no dihedral angle violation exceeding 3°. Residues 4–6 and 19–31 are well defined with r.m.s.d. values of 0.29 Å, but the sparsity of NOEs for the remaining residues, particularly residues 8–18, results in poor definition in the other regions of the molecule. The disorder for residues 8–18 appears to be a result of conformational flexibility and not just the lack of NOEs,

FIG. 3. Summary of the sequential and medium NOE connectivities for MrVIB. The chemical shift index (CSI) for each residue is shown as a bar plot, with values of ± 1 indicating a shift deviation from random coil values of greater than 0.1 ppm. Short range NOEs are shown beneath the sequence. The thickness of the filled bars indicates relative NOE intensities. The $^3J_{\text{HN-H}\alpha}$ coupling constants above 8 Hz are shown as arrows pointing upward, and those below 6 Hz are represented as arrows pointing downward. The positive ϕ angle of Phe²⁸ is represented as an open circle, and restraints of $-100^\circ \pm 80^\circ$ are shown with open triangles. Residues with χ^1 angle restraints are shown with filled squares.

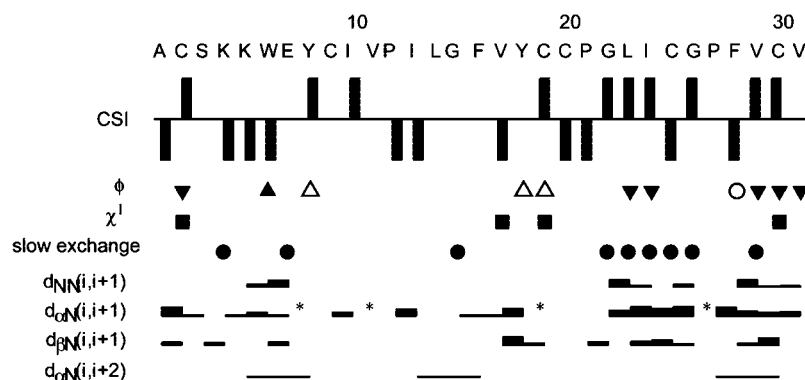


FIG. 4. Schematic diagram of the secondary structure of MrVIB showing the inter-strand NOEs (continuous arrows) and potential hydrogen bonds (broken lines). Inter-residual HN-HN, H α -HN, and H α -H α NOEs are shown with arrows. The α -carbon atoms are labeled according to their residue numbers. For clarity, sequential NOEs are omitted. The hydrogen bonds were inferred from slow exchange data and preliminary structure calculations.

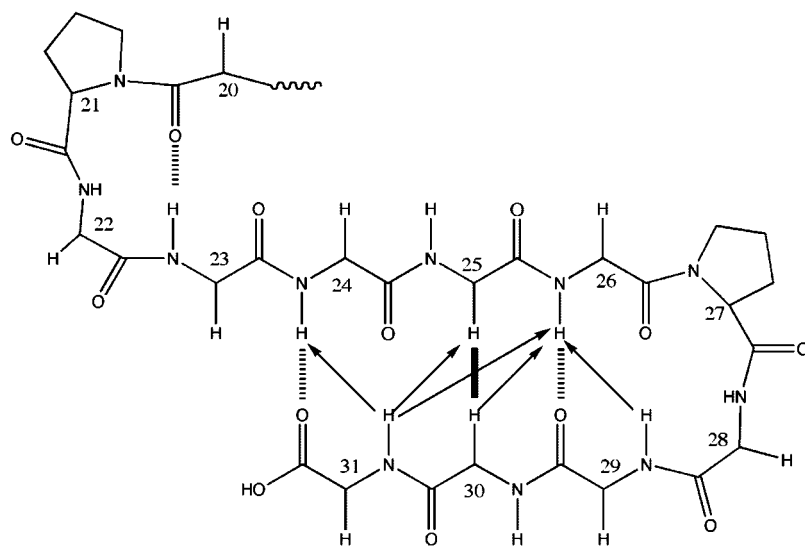
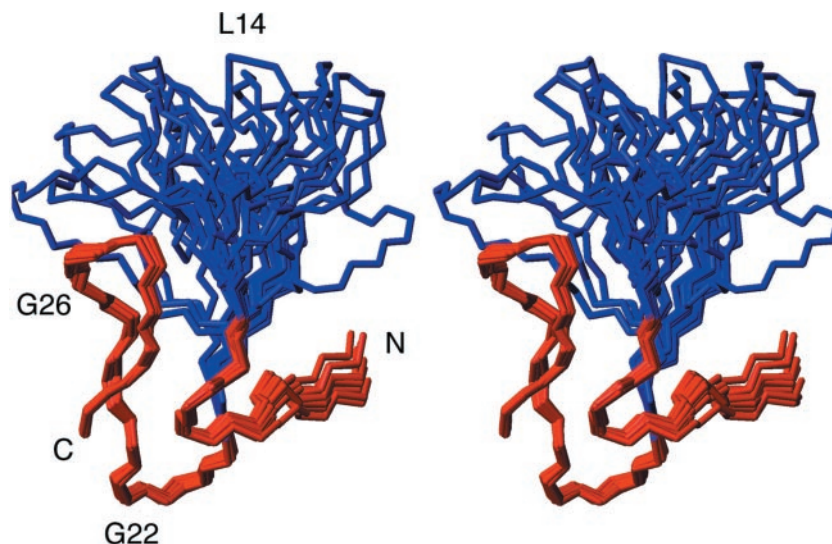


FIG. 5. The solution structure of MrVIB in 50% CD₃CN. The 20 lowest energy solution structures of MrVIB are superimposed over the backbone atoms (N, C $^{\alpha}$, and C $^{\beta}$) of residues 4–6 and 19–30 and shown in stereoscopic view. The well defined regions are shown in red, and the disordered loop corresponding to residues 7–18 is shown in blue.



based on the broadened peaks observed for several residues in this region. Fig. 6 shows a region of the NOESY spectrum highlighting the broader peaks observed for Val¹¹ and Ile¹³ compared with other peaks in the spectrum.

An analysis of the family of structures using the program PROMOTIF (20) shows that the main element of secondary structure of MrVIB is an anti-parallel β -sheet, consistent with the prediction from the NMR chemical shift, coupling, and NOE data. The strands of the β -sheet consist of residues 24–25 and 30–31 with an inverse γ turn between residues 26 and 28.

Preliminary structures were calculated without any hydrogen bond restraints, but these structures were consistent with hydrogen bonds across the β -sheet between 24 HN and 31 CO, 26 HN and 29 CO, and 31 HN and 24 CO. The latter hydrogen bond was not detected as a slow exchange amide, but this is most likely due to the low intensity of the signal due to broadening. Additional hydrogen bonds are present in several β -turns between the CO of residue i and HN of residue $i+3$. In particular, type I β -turns are present between residues 4 and 7 and between 12 and 15, and there is a type IV β -turn between

TABLE I
Structural statistics for the 20 lowest energy structures of μ O-MrVIB
The values in the table are the mean \pm S.D.

Experimental restraints	
Sequential NOEs	74
Medium range NOEs	38
Long range NOEs	77
Hydrogen bonds	10
Dihedral angles	15
Mean RMSDs from experimental restraints	
NOE distances (\AA)	0.054 ± 0.003
Dihedral angles ($^\circ$)	0.55 ± 0.14
Mean RMSDs from idealized covalent geometry	
Bonds (\AA)	0.0044 ± 0.0002
Angles ($^\circ$)	0.55 ± 0.04
Impropers ($^\circ$)	0.41 ± 0.04
Mean energies (kcal mol^{-1})	
E_{NOE}^a	27.8 ± 2.8
E_{cdih}^a	0.29 ± 0.15
E_{bond}	9.3 ± 0.87
E_{angle}	40.2 ± 5.2
E_{improper}	6.8 ± 1.3
E_{vdw}	-36.1 ± 9.9
Atomic RMSDs (\AA) ^b	
Backbone atoms (residues 4–6, 19–31)	0.29 ± 0.10
Heavy atoms (residues 4–6, 19–31)	0.68 ± 0.18
Ramachandran statistics (%) ^a	
(residues 4–6, 19–31)	
Residues in most favored regions	78.2
Residues in additional allowed regions	21.8
Residues in disallowed regions	0.0

^a Procheck_NMR was used to calculate the Ramachandran statistics.
^b Atomic r.m.s.d. values are the pairwise RMS difference for the family of structures.

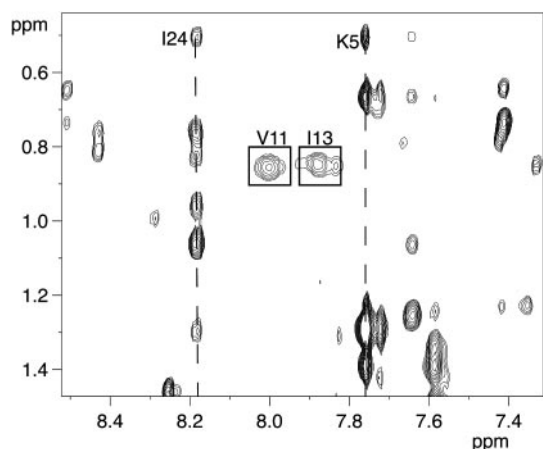


FIG. 6. Comparison of linewidths of selected peaks in a region of a NOESY spectrum of MrVIB recorded on a 750-MHz spectrometer at 290 K. The cross-peaks resulting from Val¹¹ and Ile¹³ are highlighted with boxes to indicate the increased linewidth relative to other resonances.

residues 20 and 23. The type I turn for residues 12–15 is present in a region of the molecule having very few NOEs and is consequently poorly defined. The structures also provide an explanation for the observation of a signal from the N terminus in TOCSY and NOESY spectra: 70% of the structures indicate a hydrogen bond between the amino group of Ala¹ and the hydroxyl of Tyr¹⁸.

The disulfide bonds between Cys² and Cys²⁰ and between Cys¹⁹ and Cys³⁰ are classified as right-handed hooks in a majority of the 20 final structures. The disulfide bond between residues 9 and 25 does not have a single preferred geometry throughout the structures. These structural findings are based on the assumption that the disulfide connectivity reported pre-

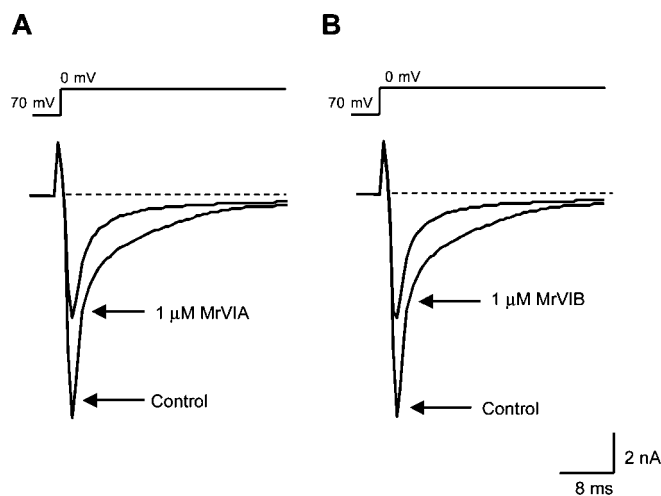


FIG. 7. Effects of μ O-conotoxins MrVIA and MrVIB on transient Na^+ currents in rat DRG neurons. Superimposed traces are shown of depolarization-activated Na^+ currents obtained in the absence (control) and presence of $1 \mu\text{M}$ MrVIA (A) and MrVIB (B). Washout of MrVIA and -B resulted in 95% recovery of peak Na^+ current amplitude. This DRG neuron exhibited largely TTX-S Na^+ current with a small component of slowly inactivating TTX-R Na^+ current.

viously (11) is correct, as seems likely, but to provide further support for this suggestion additional calculations were done with alternative connectivities. In previous studies, MrVIB was synthesized with Cys⁹ and Cys²⁵ selectively protected, and the four remaining cysteine residues were allowed to form disulfide bonds in a nonselective fashion (11). These four cysteine residues can theoretically form three connectivities, and structures were calculated with each of these connectivities, keeping the Cys⁹-Cys²⁵ bond fixed. From these studies the Cys²-Cys²⁰, Cys⁹-Cys²⁵, and Cys¹⁹-Cys³⁰ disulfide set was found to have significantly better fits to the experimental restraints. For instance, the Cys²-Cys¹⁹, Cys⁹-Cys²⁵, and Cys²⁰-Cys³⁰ connectivity had several large NOE violations, including an average violation of 0.71\AA for the NOE between Cys¹⁹ HB3 and Leu²³ HN. The χ_1 angle restraint on Cys¹⁹ also showed significant violations for this connectivity (average violation of 15°). In the Cys²-Cys³⁰, Cys⁹-Cys²⁵, and Cys¹⁹-Cys²⁰ connectivity, a large number of relatively small NOE violations were observed, and again, the Cys¹⁹ χ_1 angle restraint violated significantly (average violation of 31°) in addition to the χ_1 angle restraints of Cys² and Cys³⁰ (average violations of 6.3° and 17.1° , respectively). The connectivity pattern of Cys^I-Cys^{IV}, Cys^{II}-Cys^V, and Cys^{III}-Cys^{VI} confirmed in the current study to be present in MrVIB is the same as is seen in a range of cystine knot structures (26). Analysis of the three-dimensional structure of MrVIB suggests that the topology is that of an inhibitor cystine knot (ICK) peptide (27).

Effects of MrVIA and MrVIB on Neuronal Whole Cell Na^+ Currents—The effects of μ O-conotoxins MrVIA and MrVIB on peak TTX-R and TTX-S Na^+ currents in rat DRG neurons were investigated. Large diameter DRG neurons (capacitance 20–35 picofarads) exhibited mostly TTX-S Na^+ currents with fast activation and inactivation kinetics, whereas small (2–10 picofarads) and medium sized (10–20 picofarads) neurons exhibited both fast TTX-S and slow TTX-R Na^+ currents, similar to that described previously (28, 29). Bath application of MrVIA and MrVIB ($1 \mu\text{M}$) reversibly reduced the peak amplitude of both TTX-S ($\geq 90\%$ of current sensitive to 300 nM TTX) and TTX-R Na^+ currents in rat DRG neurons (Fig. 7). Concentration-response curves indicated that MrVIA and MrVIB exhibit a similar potency, however, given that MrVIA was more readily available than MrVIB, MrVIA was used for further experi-

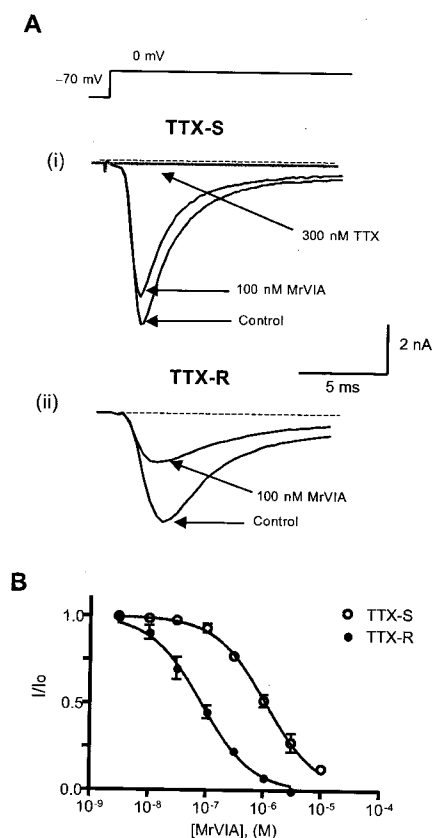


FIG. 8. Effects of MrVIA on TTX-sensitive and TTX-resistant Na⁺ currents in rat DRG neurons. In *A*: *i*, superimposed traces of Na⁺ currents recorded from a DRG neuron exhibiting only fast, TTX-S Na⁺ current. Depolarization-activated Na⁺ currents were obtained in the absence (control) and presence of 100 nM MrVIA and were completely blocked by 300 nM TTX. *ii*, superimposed Na⁺ currents recorded from a different DRG neuron in the presence of 300 nM TTX (TTX-resistant Na⁺ current) in the absence (control) and presence of 100 nM MrVIA. *B*, neurons exhibiting Na⁺ current that was abolished by 300 nM TTX ($\geq 90\%$) were used for comparison of toxin affinity on TTX-R versus TTX-S Na⁺ current. The half-maximal inhibitory concentration (IC₅₀) for the TTX-R Na⁺ current was 82.8 nM ($n = 7$) and 1.02 μ M ($n = 7$) for the TTX-S Na⁺ current.

ments. MrVIA was found to have a 10-fold higher affinity for inhibition of TTX-R than TTX-S Na⁺ currents in rat DRG neurons (Fig. 8, *A* and *B*). The half-maximal inhibitory concentration (IC₅₀) for reduction of peak TTX-R Na⁺ current was 82.8 nM ($n = 7$) and 1.02 μ M ($n = 7$) for the TTX-S Na⁺ current (Fig. 8*B*). The kinetics of onset and recovery from block by MrVIA are shown for TTX-R and TTX-S Na⁺ currents in Fig. 9. From this experiment, the K_d for the TTX-R Na⁺ current was 82 and 647 nM for the TTX-S Na⁺ current. The off-rate was relatively similar for TTX-R versus TTX-S Na⁺ current, and K_d was determined largely by the ~ 10 -fold difference in on-rate. In addition, MrVIA did not change the current-voltage relationship for either TTX-R or TTX-S Na⁺ current (Fig. 10). In a series of experiments to examine the effect of MrVIA on voltage-dependent Ca²⁺ channels, MrVIA at concentrations of up to 10 μ M had no effect on depolarization-activated Ba²⁺ current amplitude in rat DRG neurons ($n = 6$) as shown in Fig. 11.

DISCUSSION

In this study, we have determined for the first time the three-dimensional structure adopted by μ O-conotoxins and established that members of this class act at a mammalian TTX-R sodium channel. The μ O-conotoxins MrVIA and MrVIB were found to inhibit both TTX-S and TTX-R Na⁺ currents in rat DRG neurons, with IC₅₀ values of ~ 1 μ M and ~ 80 nM,

respectively. The IC₅₀ value for TTX-R Na⁺ currents is very similar to that reported previously for inhibition of Na⁺ currents in molluscan neurons (11, 13), whereas the IC₅₀ value for TTX-S Na⁺ currents is ~ 10 times higher. The binding site for MrVIA/B on the VSSC is currently unknown but is distinct from site 1 where μ -conotoxins bind (12).

The transient TTX-R Na⁺ current in DRG neurons appears to be mediated by the Na_v1.8/PN3/SNS VSSC subtype (31, 32). Na_v1.8 is expressed almost exclusively in small and medium sized DRG neurons, most of which are nociceptors (33, 34), and is up-regulated in inflammatory pain states (35, 36). The role of Na_v1.8 in pain was confirmed by studies of Na_v1.8 null mutant mice, which exhibited a decreased response to noxious mechanical stimuli and reduced inflammatory-induced hyperalgesia (3). These observations suggest that selective inhibition of Na_v1.8 could produce analgesia without side-effects (37–40). The μ O-conotoxins, MrVIA and MrVIB, are the first known peptide inhibitors of the mammalian TTX-R Na⁺ current in DRG neurons, and it is possible that engineering of these toxins could produce the first selective inhibitors for TTX-R Na⁺ channels.

Analysis of the structures of the μ O-conotoxins has revealed some interesting features that may have functional significance. Both MrVIA and MrVIB aggregate in aqueous solution at millimolar concentrations, based on the very broad signals observed in the NMR spectra. This finding is consistent with the late elution time on HPLC of these peptides and their high content of hydrophobic residues. Although the peptides visually appear to be soluble in aqueous solution, the broad NMR peaks suggest that they are highly aggregated. Certainly, dimers or small oligomers would not be expected to result in the degree of broadening observed. The presence of organic solvent, in particular acetonitrile, substantially improved the quality of the spectra, presumably by stabilizing a monomeric conformation.

The main element of secondary structure in MrVIB is a small region of β -sheet between residues 24 and 25 and between 30 and 31. The β -sheet is stabilized by hydrogen bonds between 24 HN and 31 CO, 26 HN and 29 CO, and 31 HN and 24 CO. Additional hydrogen bonds are also present to stabilize several β -turns in MrVIB, as well as to stabilize the N terminus. Unusually, a signal from the N-terminal amino group is present in the TOCSY and NOESY spectra. The unusually slow exchange of the N-terminal amine appears to be the result of a hydrogen bond with the hydroxyl of Tyr¹⁸.

Both strands involved in the β -sheet of MrVIB contain cysteine residues that form disulfide bonds and connect the strands to other regions, forming a compact core in the molecule. The disulfide connectivity was previously established using synthetic methods to be Cys²-Cys²⁰, Cys⁹-Cys²⁵, and Cys¹⁹-Cys³⁰ (11). The NMR data in the current study have confirmed this connectivity but also show that the disulfide bonds are topologically arranged to form an ICK motif (27). This motif involves the disulfide bonds between Cys² and Cys²⁰ and between Cys⁹ and Cys²⁵ and their connecting backbone segments forming a ring through which the Cys¹⁹ to Cys³⁰ disulfide bond threads. The knotted structure is likely to play a significant role in stabilizing the overall fold.

The ICK motif is now known to be present in a variety of proteins, many of which are toxins (26, 27). In particular, both the ω - and δ -conotoxins contain a cystine knot motif (41, 42), and a comparison of the structures of members of these families with MrVIB is shown in Fig. 9. The overall fold is maintained in all three families despite the sequence variation, suggesting a crucial role for the disulfide bonds in maintaining the structure. Other studies on cystine knot proteins have also high-

FIG. 9. Time course of onset and recovery from block of depolarization-activated TTX-sensitive and TTX-resistant Na⁺ currents by MrVIA. *A*, the relative peak Na⁺ current amplitude plotted as a function of time during bath application of 100 and 300 nM MrVIA and upon washout. TTX-R Na⁺ current was recorded in the presence of 300 nM TTX ($n = 4$). Representative TTX-R Na⁺ currents corresponding to those elicited before and during the onset and recovery from block are shown below. *B*, the relative peak TTX-sensitive Na⁺ current amplitude plotted as a function of time during bath application of 1 μ M MrVIA and upon washout ($n = 3$). Error bars (\pm S.E.) are obscured by the data points. Representative TTX-S Na⁺ currents recorded at different times before and during the onset and recovery from block are shown below. From estimates of on- and off-rates the K_d for inhibition of the TTX-R Na⁺ current was 82 nM and for the TTX-S Na⁺ current was 647 nM.

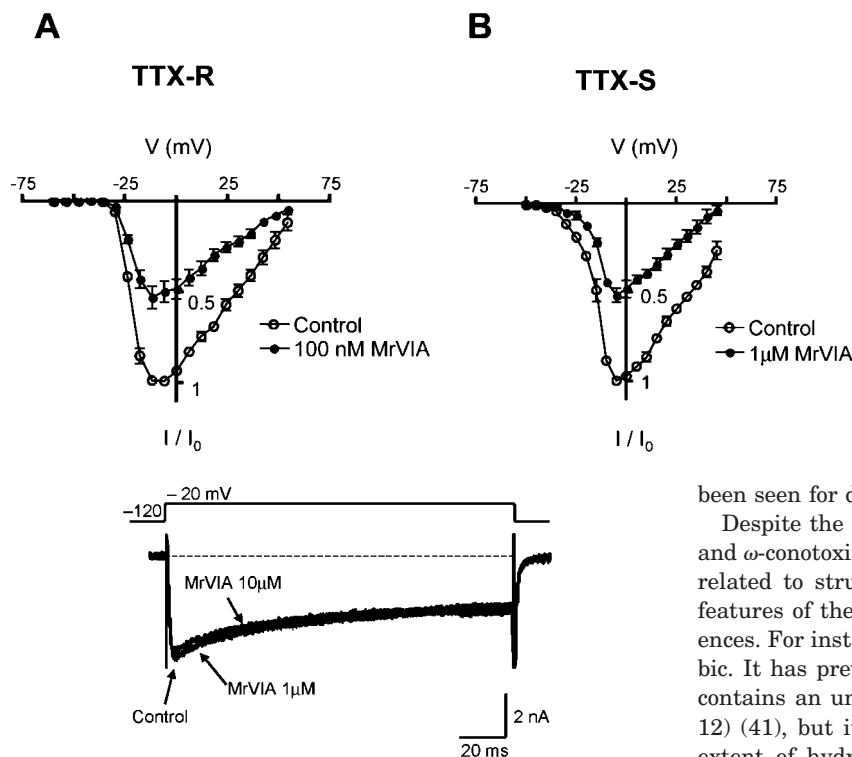
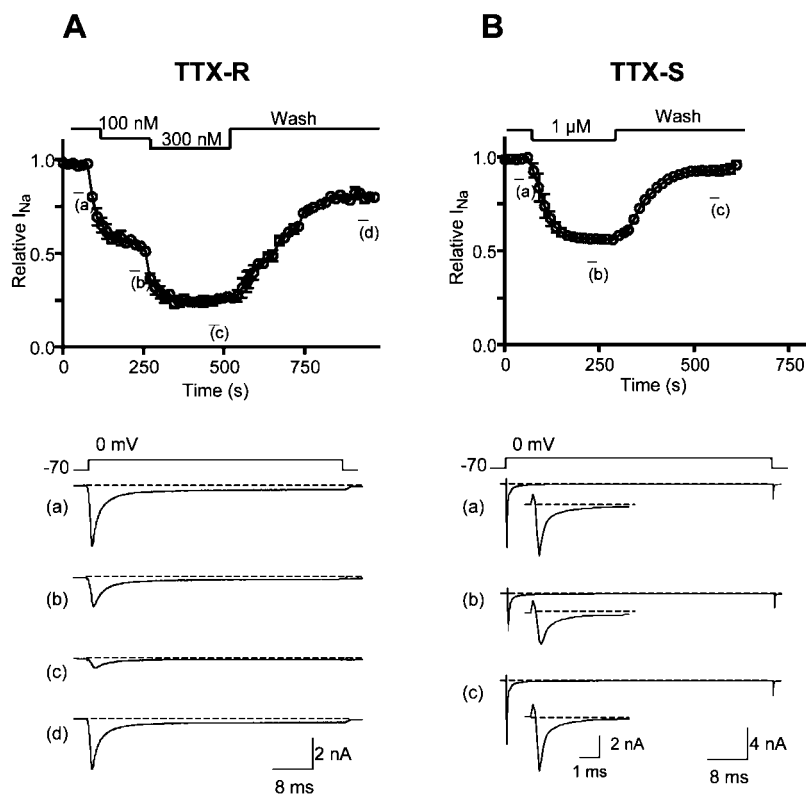


FIG. 11. Depolarization-activated Ca²⁺ channel currents in DRG neurons are insensitive to MrVIA. Superimposed Ba²⁺ currents in response to step depolarization from -120 mV to -20 mV obtained in the absence (control) and presence of 1 μ M and 10 μ M MrVIA. Depolarization-activated Ba²⁺ currents were recorded in a Na⁺-free extracellular solution containing 4 mM Ba²⁺.

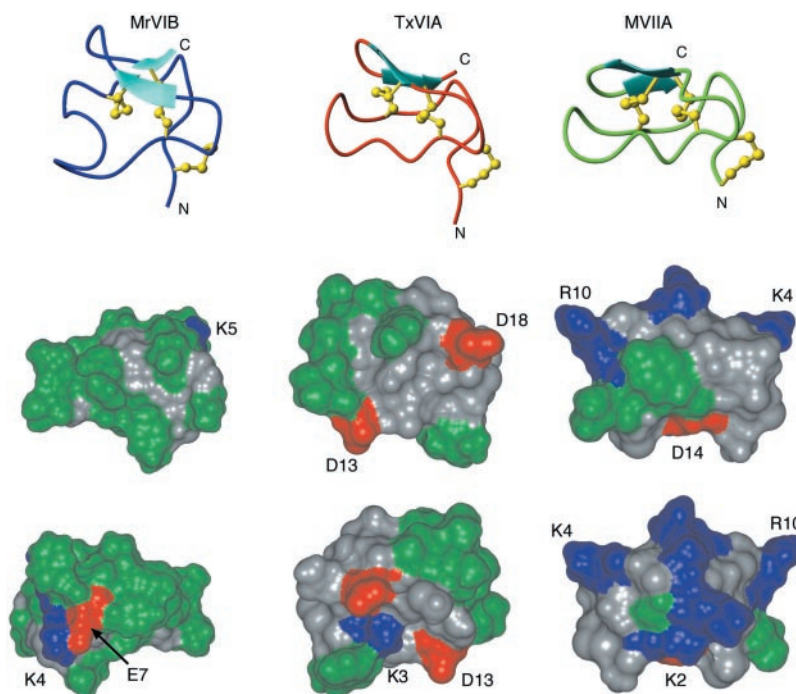
lighted the importance of the disulfide bonds. For example, the structures of disulfide isomers of ω -conotoxin GVIA differ significantly from the native structure and have no activity at the N-type calcium channel (43). Variations in activity have also

FIG. 10. Current-voltage relationships of TTX-R (A) and TTX-S (B) Na⁺ currents obtained in the absence (control) and presence of MrVIA. TTX-R Na⁺ currents recorded in the presence of 300 nM TTX were inhibited by 100 nM MrVIA, whereas TTX-S Na⁺ currents were inhibited by 1 μ M MrVIA.

been seen for disulfide bond isomers of α -conotoxins (44, 45).

Despite the structural similarities observed for the μ O-, δ -, and ω -conotoxins, they clearly act in distinct ways that must be related to structural differences. An analysis of the surface features of the peptides shown in Fig. 12 reveals such differences. For instance, most of the surface of MrVIB is hydrophobic. It has previously been noted that the δ -conotoxin TxVIA contains an unusual surface-exposed hydrophobic patch (Fig. 12) (41), but it is apparent from the present study that the extent of hydrophobicity is quite different from μ O-MrVIB. This is reflected in the differing aggregation states of the peptides. The three-dimensional structure of TxVIA was determined in aqueous solution at a quite high concentration (\sim 5 mM (41)), whereas MrVIA and MrVIB appear to aggregate in aqueous solution at much lower concentrations (\sim 1 mM). Both TxVIA and MVIIA have a larger number of hydrophilic and charged residues than MrVIB, and this is highlighted in Fig. 12. The hydrophobic patch of TxVIA has been implicated in playing an important role in binding to sodium channels. MrVIB has a hydrophobic patch in a similar location but, as

FIG. 12. Comparison of the structures of μ O-MrVIB (this study), δ -TxVIA (41), and ω -MVIIA (42) aligned over the backbone atoms of the cysteine residues. Ribbon representations are shown with the β -strands as arrows and the disulfide bonds in a ball-and-stick format. Surface representations of each molecule are shown under the ribbon diagrams in two views (the lower view rotated 180° about the z-axis relative to the other view). Hydrophobic residues are shown in green, positively charged in blue, and negatively charged in red. The remaining residues are shown in gray. Selected charged residues are labeled with the single-letter amino acid codes. The hydrophobic patch in δ -TxVIA implicated in binding to sodium channels is on the left side of this upper surface diagram.



mentioned above, also has a large number of other surface-exposed hydrophobic residues, and therefore it is difficult to predict if this particular region plays a role in binding to the receptor. Mutagenesis studies will be necessary to elucidate the importance of various surface residues.

The most striking difference between MrVIB and the ω - and δ -conotoxins is the disorder observed in loop 2 of MrVIB. Relaxation experiments will be required to determine if this disorder is a result of structural flexibility or if indeed the aggregation observed in aqueous solution that appears to be modulated by acetonitrile is responsible for the disorder. Such a disordered loop is unprecedented in the O superfamily conotoxins, although a limited degree of flexibility has been reported for loop 2 of the ω -conotoxin MVIIA. In that case, it is known that loop 2 is critical for high affinity binding to voltage-gated calcium channels. Broadening of peaks from residues 11–13 suggested slow conformational exchange (42), and this was also supported by NMR relaxation measurements (46). It has been suggested that this conformational exchange may have functional significance and may allow MVIIA to bind to two different receptor subtypes in the molluscs that it preys upon (46).

Flexibility in proteins is increasingly being taken into account in drug design applications, because disordered regions can allow variability in protein recognition motifs, permitting a given sequence to adaptively recognize multiple binding partners (47). The apparent flexibility observed in the structure of MrVIB reported here may have implications for its cross-channel activity at the mollusc neuronal sodium and calcium channels in addition to activity at both TTX-R and TTX-S mammalian sodium channels.

The unusual cross channel activity at both sodium and calcium channels in molluscan neurons has been observed in at least three other peptide toxins, namely the tarantula peptides ProTx-I and ProTx-II (48) and the α -scorpion-toxin-like peptide, kurtoxin (49). The only sequence conservation between these peptides and MrVIA/MrVIB is the high content of cysteine residues, with the ProTx peptides containing six cysteine residues and kurtoxin containing eight. The disulfide connectivity has been elucidated for the ProTx peptides and shown to be Cys^I-Cys^{IV}, Cys^{II}-Cys^V, and Cys^{III}-Cys^{VI} (48). It has been

suggested that they contain an inhibitor cystine knot motif based on this connectivity. Because the three-dimensional structures of these toxins have not been reported, it remains to be seen if structural flexibility is also a distinguishing feature of these toxins. Structural analysis may assist in determining key features of these toxins that interact with both sodium and calcium channels. Other peptide toxins containing a cystine knot motif that have been implicated in sodium channel activity include GS (50) and TVIIA (30).

In summary, we have shown MrVIA and MrVIB to be the first peptidic inhibitors of the transient TTX-R Na⁺ current in rat DRG neurons. The equivalent ion channels in humans are therapeutic targets for the treatment of pain. Furthermore, we have used NMR spectroscopy to provide the first structural information on this class of conotoxins. A disordered loop 2 in the structure of MrVIB is likely to result from structural flexibility and may allow binding to calcium and TTX-R and TTX-S sodium channels. However, structure activity studies are required to provide information on the importance of particular residues in binding to these different ion channels.

Acknowledgment—We thank Dr. Leonid Motin for assistance with the electrophysiological experiments.

REFERENCES

- Adams, D. J., Alewood, P. F., Craik, D. J., Drinkwater, R. D., and Lewis, R. J. (1999) *Drug Dev. Res.* **46**, 219–234
- Jones, R. M., and Bulaj, G. (2000) *Curr. Pharm. Des.* **6**, 1249–1285
- Akopian, A. N., Souslova, V., England, S., Okuse, K., Ogata, N., Ure, J., Smith, A., Kerr, B. J., McMahon, S. B., Boyce, S., Hill, R., Stanfa, L. C., Dickenson, A. H., and Wodd, J. N. (1999) *Nat. Neurosci.* **2**, 541–548
- Eglen, R. M., Hunter, J. C., and Dray, A. (1999) *Trends Pharmacol. Sci.* **20**, 337–342
- Porreca, F., Lai, J., Bian, D., Wegert, S., Ossipov, M. H., Eglen, R. M., Kassotakis, L., Novakovic, S., Rabert, D. K., Sangameswaran, L., and Hunter, J. C. (1999) *Proc. Natl. Acad. Sci. U. S. A.* **96**, 7640–7644
- Coward, K., Plumpton, C., Facer, P., Birch, R., Carlstedt, T., Tate, S., Bountra, C., and Anand, P. (2000) *Pain* **85**, 41–50
- Taylor, C. P., and Meldrum, B. S. (1995) *Trends Pharmacol. Sci.* **16**, 309–316
- Carter, A. J. (1998) *Amino Acids* **14**, 159–169
- Ragsdale, D. S., and Avoli, M. (1998) *Brain Res. Brain Res. Rev.* **26**, 16–28
- Rho, J. M., and Sankar, R. (1999) *Epilepsia* **40**, 1471–1483
- McIntosh, J. M., Hasson, A., Spira, M. E., Gray, W. R., Li, W., Marsh, M., Hillyard, D. R., and Olivera, B. M. (1995) *J. Biol. Chem.* **270**, 16796–16802
- Terlau, H., Stocker, M., Shon, K. J., McIntosh, J. M., and Olivera, B. M. (1996) *J. Neurophysiol.* **76**, 1423–1429
- Fainzilber, M., R., v. d. S., Lodder, J. C., Li, K. W., Geraerts, W. P., and Kits, K. S. (1995) *Biochemistry* **34**, 5364–5371

14. Piatto, M., Saudek, V., and Sklenar, V. (1992) *J. Biomol. NMR* **2**, 661–665
15. Rosengren, K. J., Daly, N. L., Plan, M. R., Waine, C., and Craik, D. J. (2003) *J. Biol. Chem.* **278**, 8606–8616
16. Brünger, A. T., Adams, P. D., and Rice, L. M. (1997) *Structure* **5**, 325–336
17. Rice, L. M., and Brünger, A. T. (1994) *Proteins* **19**, 277–290
18. Stein, E. G., Rice, L. M., and Brünger, A. T. (1997) *J. Magn. Reson.* **124**, 154–164
19. Linge, J. P., and Nilges, M. (1999) *J. Biomol. NMR* **13**, 51–59
20. Hutchinson, E. G., and Thornton, J. M. (1996) *Protein Sci.* **5**, 212–220
21. Laskowski, R. A., Rullmann, J. A., MacArthur, M. W., Kaptein, R., and Thornton, J. M. (1996) *J. Biomol. NMR* **8**, 477–486
22. Wüthrich, K. (1986) *NMR of Proteins and Nucleic Acids*, Wiley-Interscience, New York
23. Wishart, D. S., Sykes, B. D., and Richards, F. M. (1992) *Biochemistry* **31**, 1647–1651
24. Wishart, D. S., Bigam, C. G., Holm, A., Hodges, R. S., and Sykes, B. D. (1995) *J. Biomol. NMR* **5**, 67–81
25. Dyson, H. J., Rance, M., Houghten, R. A., Lerner, R. A., and Wright, P. E. (1988) *J. Mol. Biol.* **201**, 161–200
26. Craik, D. J., Daly, N. L., and Waine, C. (2001) *Toxicol.* **39**, 43–60
27. Pallaghy, P. K., Nielsen, K. J., Craik, D. J., and Norton, R. S. (1994) *Protein Sci.* **3**, 1833–1839
28. Elliott, A. A., and Elliott, J. R. (1993) *J. Physiol.* **463**, 39–56
29. Rush, A. M., Brau, M. E., Elliott, A. A., and Elliott, J. R. (1998) *J. Physiol.* **511** (Pt 3), 771–789
30. Hill, J. M., Alewood, P. F., and Craik, D. J. (2000) *Eur. J. Biochem.* **267**, 4649–4657
31. Cummins, T. R., Black, J. A., Dib-Hajj, S. D., and Waxman, S. G. (2000) *J. Neurosci.* **20**, 8754–8761
32. Sangameswaran, L., Delgado, S. G., Fish, L. M., Koch, B. D., Jakeman, L. B., Stewart, G. R., Sze, P., Hunter, J. C., Eglén, R. M., and Herman, R. C. (1996) *J. Biol. Chem.* **271**, 5953–5956
33. Rabert, D. K., Koch, B. D., Inicka, M., Obernolte, R. A., Naylor, S. L., Herman, R. C., Eglén, R. M., Hunter, J. C., and Sangameswaran, L. (1998) *Pain* **78**, 107–114
34. Fjell, J., Hjelmstrom, P., Hormuzdiar, W., Milenkovic, M., Aglieco, F., Tyrrell, L., Dib-Hajj, S., Waxman, S. G., and Black, J. A. (2000) *Neuroreport* **11**, 199–202
35. Shembalkar, P. K., Till, S., Boettger, M. K., Terenghi, G., Tate, S., Bountra, C., and Anand, P. (2001) *Eur. J. Pain* **5**, 319–323
36. Tanaka, M., Cummins, T. R., Ishikawa, K., Dib-Hajj, S. D., Black, J. A., and Waxman, S. G. (1998) *Neuroreport* **9**, 967–972
37. Brock, J. A., McLachlan, E. M., and Belmonte, C. (1998) *J. Physiol.* **512** (Pt 1), 211–217
38. Lai, J., Gold, M. S., Kim, C. S., Bian, D., Ossipov, M. H., Hunter, J. C., and Porreca, F. (2002) *Pain* **95**, 143–152
39. Saab, C. Y., Cummins, T. R., Dib-Hajj, S. D., and Waxman, S. G. (2002) *Neurosci. Lett.* **331**, 79–82
40. Scholz, A., and Vogel, W. (2000) *Pain* **89**, 47–52
41. Kohno, T., Sasaki, T., Kobayashi, K., Fainzilber, M., and Sato, K. (2002) *J. Biol. Chem.* **277**, 36387–36391
42. Nielsen, K. J., Thomas, L., Lewis, R. J., Alewood, P. F., and Craik, D. J. (1996) *J. Mol. Biol.* **263**, 297–310
43. Flinn, J. P., Pallaghy, P. K., Lew, M. J., Murphy, R., Angus, J. A., and Norton, R. S. (1999) *Biochim. Biophys. Acta* **1434**, 177–190
44. Gehrmann, J., Alewood, P. F., and Craik, D. J. (1998) *J. Mol. Biol.* **278**, 401–415
45. Dutton, J. L., Bansal, P. S., Hogg, R. C., Adams, D. J., Alewood, P. F., and Craik, D. J. (2002) *J. Biol. Chem.* **277**, 48849–48857
46. Atkinson, R. A., Kieffer, B., Dejaegere, A., Sirockin, F., and Lefevre, J. F. (2000) *Biochemistry* **39**, 3908–3919
47. Teague, S. J. (2003) *Nat. Rev. Drug Discov.* **2**, 527–541
48. Middleton, R. E., Warren, V. A., Kraus, R. L., Hwang, J. C., Liu, C. J., Dai, G., Brochu, R. M., Kohler, M. G., Gao, Y. D., Garsky, V. M., Bogusky, M. J., Mehl, J. T., Cohen, C. J., and Smith, M. M. (2002) *Biochemistry* **41**, 14734–14747
49. Chuang, R. S., Jaffe, H., Cribbs, L., Perez-Reyes, E., and Swartz, K. J. (1998) *Nat. Neurosci.* **1**, 668–674
50. Hill, J. M., Alewood, P. F., and Craik, D. J. (1997) *Structure* **5**, 571–583